2.G

Nuclear Physics A273 (1976) 69—94; © *North-Holland Publishing Co., Amsterdam*

INELASTIC PROCESSES AND FORM FACTOR EFFECTS IN THE ^{162,164}Dy(^{3}He, d) REACTIONS AT 46.5 MeV†

A. S. BROAD††, D. A. LEWIS††† and W. S. GRAY

Cyclotron Laboratory, Physics Department, The University of Michigan, Ann Arbor, Michigan 48109

and

P. J. ELLIS and A. DUDEK-ELLIS

Nuclear Physics Laboratory, Oxford, UK

and

School of Physics and Astronomy, University of Minnesota, Minneapolis, Minnesota 55455‡

Received 29 August 1975

(Revised 23 June 1976)

Abstract: The ^{162,164}Dy(^{3}He, d) reactions at $E_{^3He}$ = 46.5 MeV are analyzed using the coupled channels Born approximation (CCBA) and improved form factors derived from a deformed Woods-Saxon potential. The latter are generated using the coupled channels procedure of Rost. The transitions considered populate the $\frac{7}{2}^-$[523], $\frac{1}{2}^+$[411], $\frac{3}{2}^+$[411], $\frac{1}{2}^-$[541] and $\frac{5}{2}^+$[402] orbitals in ^{163,165}Ho. Indirect processes induced by inelastic scattering are found to have an influence on the cross sections comparable to that deduced for neutron transfer reactions on rare earth nuclei at lower energies. Considered alone, these can alter the cross sections even of strong transitions by a factor of two and of weaker ones by an order of magnitude. For the weaker transitions equally large changes can result when the improved form factors, rather than conventional spherical Woods-Saxon functions, are used in the calculations. In the examples considered these two effects tend to cancel, often, but not always, resulting in predicted cross sections similar in magnitude to the results of conventional DWBA calculations made with spherical Woods-Saxon form factors. The CCBA angular distributions are generally similar in shape to DWBA predictions, which usually give good fits to the experimental angular distributions over the 0–35° range of the data. Compared with DWBA predictions which use the same optical parameters, but spherical Woods-Saxon form factors, the CCBA with deformed Woods-Saxon form factors is in better overall agreement with the experimental cross-section magnitudes. However there are a number of cases in which the CCBA, although usually predicting larger cross sections than the DWBA, still underestimates the experimental cross sections by nearly factor of two. These cases all occur in the $\frac{1}{2}^-$[541] band or in the strongly Coriolis mixed $\frac{1}{2}^+$[411] and $\frac{3}{2}^+$[411] bands, and include the majority of transitions populating these orbitals. Since both nuclear structure and reaction mechanism effects are interwoven in the calculations, further data would be most useful in probing the origin of the discrepancy.

E NUCLEAR REACTIONS ^{162,164}Dy(^{3}He, d), E = 46.5 MeV; calculated $\sigma(E_d, \theta)$. ^{163,165}Ho levels deduced form factors. CCBA, DWBA analysis.

† Work supported in part by the US Energy Research and Development Administration.

†† Present address: LeCroy Research Systems Corp., 126 North Route 303, West Nyack, New York 10994.

††† Present address: J. H. Williams Laboratory, University of Minnesota, Minneapolis, Minnesota 55455.

‡ Present address.

1. Introduction

Over the last decade single-nucleon transfer reactions such as (d, p) or (^{3}He, d) have been used extensively to study the one-quasiparticle excitations of heavy, deformed nuclei. These reactions have usually been analyzed assuming that the distorted-wave Born approximation (DWBA) gives an adequate account of the reaction, and that a spherical Woods-Saxon well can be used to generate the radial wave function for the transferred particle.

This reaction model, if valid, has the attractive feature that the different angular momentum components of a given one-quasiparticle intrinsic state χ_Ω can be determined by measuring the relative cross sections for populating, in an odd-A nucleus, the corresponding members of the rotational band based on that state. Thus if χ_Ω is expanded on a spherical basis as

$$\chi_\Omega = \sum_{lj} C_{lj}\varphi_{Nlj\Omega}, \tag{1.1}$$

the cross section for populating the spin-j member of the band becomes [1])

$$\frac{d\sigma}{d\Omega} = 2C_{lj}^2 \begin{Bmatrix} U^2 \\ V^2 \end{Bmatrix} \sigma_{lj}(\theta), \tag{1.2}$$

where U^2 and V^2 are the usual BCS model occupation probabilities appropriate for stripping or pickup reactions respectively, and $\sigma_{lj}(\theta)$ is the reduced cross section calculated with the DWBA.

Numerous band assignments have been made by comparing the "fingerprint" distribution of the C_{lj}^2 obtained from this procedure with the predictions of the Nilsson model. The results have generally been in at least qualitative agreement with Nilsson model expectations, and in many cases the agreement is very detailed [2]). This empirical success has tended to bolster confidence in the validity of the reaction model and encouraged the invocation of such refinements as Coriolis coupling or other types of band mixing in cases where discrepancies have appeared.

However, the reaction model outlined above is based on assumptions which are not necessarily justified for reactions on deformed nuclei. There is considerable evidence, to be discussed below, that its success is at least partly illusory. A key assumption of the model, which is implicit in the use of the DWBA, is that of a one-step reaction mechanism with the core remaining inert during the transfer process. Multistep processes involving both inelastic scattering and particle transfer are ignored, although for deformed targets the former would be expected to be particularly important because of the strong coupling between the elastic channel and low-lying rotational states.

A model for treating these indirect processes was proposed some time ago by Penney and Satchler [3]) who suggested that the elastic scattering wave functions appearing in the DWBA be replaced by coupled channel wave functions which contain both elastic and inelastic scattering components. This generalization is

often referred to as the coupled channels Born approximation (CCBA). An alternative, but equivalent, approach called the source term method has been described by Ascuitto and Glendenning [4]) and by Edens [5]); this approach is actually used in the present calculations.

A number of calculations have now been carried out for one nucleon transfer reactions, e.g. refs. [6-11]). Regarding the rare-earth region, the calculations to date [refs. [8-11])] have studied the (d, p) and (p, d) reactions in the 10–20 MeV range. For these reactions the CCBA predictions sometimes differ by a factor of two in magnitude from the DWBA, even for fairly strong transitions, and often by an order of magnitude for the weaker ones. In addition, there are cases in which the measured angular distributions, although fit well by the CCBA, differ drastically from the DWBA predictions [10,11]). This would tend to increase the uncertainty of spectroscopic strengths deduced from the usual procedure, since in many experiments the cross sections were measured at only a few angles. Thus there is good reason to doubt the quantitative accuracy of spectroscopic information obtained with the DWBA model, at least under the reaction conditions which have been examined.

Although one might expect similar effects to appear in proton transfer reactions in the rare-earth region, the influence of indirect processes on these reactions has not yet been investigated. Much less data are available for (d, ^{3}He) and (^{3}He, d) reactions on rare-earth targets; in particular there have been few angular distribution measurements. Recently, however, Lewis *et al.* [12]) have published data for the (^{3}He, d) reaction on ^{162,164}Dy at 46.5 MeV which include angular distributions measured for members of several different rotational bands in each residual nucleus. In ref. [12]) these reactions were analyzed using the conventional DWBA, which with only a few exceptions reproduced the measured angular distributions and yielded spectroscopic factors in qualitative agreement with the Nilsson model. One of the purposes of the present paper is to assess, using the CCBA, the importance of multistep processes in these reactions, which fall into a different projectile and energy regime than has so far been examined.

There is another feature of the usual analysis of transfer reactions on deformed nuclei which introduces additional uncertainties in the nuclear structure information which is obtained. This is the well-known inconsistency in the treatment of the radial wave function of the transferred particle, the form factor in a zero-range calculation. In the Nilsson model the eigenfunctions χ_Ω of the deformed potential are expanded on a basis of spherical harmonic oscillator functions. However, in reaction calculations these functions are ordinarily replaced by the eigenfunctions of a spherical Woods-Saxon well. Thus the basis used in the reaction calculation is not at all the same as that of the Nilsson model with which the reactions are compared. Since the various shell-model basis states appearing in a given deformed state are usually bound by quite different energies in a spherical potential, this procedure would cause the corresponding form factors to have the wrong slope in the exponential tail region where most contributions to the reactions originate. To compensate for this deficiency,

it is customary to adjust for each transition separately the well depth in such a way as to reproduce the observed separation energy. The separation energy procedure ensures that in the tail region the form factor will have the proper slope, but not necessarily the correct normalization. The error in the latter would be expected to be greatest for basis states which in the spherical limit lie far away in energy from the deformed state, i.e., for transitions to band members with small Nilsson coefficients. Since it is in these weaker transitions that indirect processes also tend to be more important, a realistic evaluation of these processes should also include more realistic form factors than the conventional ones.

Prescriptions for generating more accurate form factors appropriate for deformed orbitals have been reported in the literature [9, 13, 14]). In the scheme of Rost [14]), they are obtained by solving a coupled channel eigenvalue problem subject to the constraint that the energy eigenvalue match the separation energy of the transferred particle. In our analysis of the $^{162, 164}$Dy(^{3}He, d) reactions we have used this procedure while employing the CCBA to take into account inelastic coupling in the entrance and exit channels. In comparison with conventional DWBA predictions, we find that the modifications resulting from use of improved form factors are often comparable in magnitude to inelastic effects.

2. CCBA calculations

As we have remarked, we use the source term method [4, 5]) to incorporate inelastic scattering processes in the reaction calculations. For the present (^{3}He, d) reactions this involves solving first the coupled equations for ^{3}He elastic and inelastic scattering in the entrance channel subject to the boundary condition that incoming waves exist only in channels with the target nucleus in its ground state. The resulting wave functions are then used to construct the source term which gives the feeding of the various levels in the residual nucleus due to the stripping process. A zero range interaction is assumed with strength taken from ref. [15]). In terms of the reduced cross sections calculated with DWBA code DWUCK [16]), this strength corresponds to a "normalization factor" for the (^{3}He, d) reaction of 4.42. The source term is inserted into the coupled equations representing the scattering of deuterons from the residual nucleus and the set of inhomogeneous coupled equations solved subject to the boundary condition that there are only outgoing waves. The matching of the wave functions onto the asymptotic forms yields the scattering matrix elements in the usual way. Such a CCBA calculation takes into account inelastic scattering to all orders, but the transfer process is assumed to be sufficiently weak that it can be treated in first order only.

Firstly we need to specify the parameters which describe the elastic and inelastic scattering in the entrance and exit channels. The particle-nucleus interaction was represented by the deformed optical model potential

$$V(r,\theta) = Vf(r, R_V, a_V)+i[Wf(r, R_W, a_W)+W'g(r, R_W, a_W)]+V_{\mathrm{Coul}}(r, R_C), \quad (2.1)$$

where

$$f(r, R_k, a_k) = -(1+E_k)^{-1},$$
$$g(r, R_k, a_k) = -4E_k(1+E_k)^{-2}, \quad (2.2)$$
$$E_k = \exp[(r-R_k)/a_k].$$

The deformed surface of the optical potential is given by

$$R_k(\theta') = \bar{R}_k[1+\beta_2 Y_{20}(\theta')+\beta_4 Y_{40}(\theta')], \quad (2.3)$$

where the primes refer to the body fixed axes and $\bar{R}_k = r_C A^{\frac{1}{3}}$. The Coulomb potential was taken to be that of a uniform charge distribution with radius $r_C A^{\frac{1}{3}}$ and was also allowed to deform. No spin-orbit potential was used so that the coupled channel solutions are independent of the spin of the scattered particle. This simplifying feature makes the CCBA calculations tractable. The coupling terms were evaluated using nuclear wave functions taken from the macroscopic rotational model (with a single particle beyond the deformed core in the case of the residual odd-A nuclei).

TABLE 1

Parameters of the deformed optical model potentials

Particle	V (MeV)	r_V (fm)	a_V (fm)	W (MeV)	W' (MeV)	r_W (fm)	a_W (fm)	β_2	β_4	r_C (fm)
^{3}He	175	1.14	0.723	17.5	0	1.60	0.90	0.28	0	1.4
d	91	1.16	0.830	0	14.25	1.25	0.90	0.28	0	1.3

The optical model parameters used are given in table 1. Although these parameters originate from work in the lead region [17,18]) it was found in ref. [12]) that they also give a good account of elastic and inelastic scattering of 46.5 MeV ^{3}He ions from ^{162}Dy and 34.5 MeV deuterons from ^{166}Er, when used in coupled channels calculations which employ the deformed potential (2.1). Most of these scattering data and their analysis were presented in ref. [12]). The results are summarized in figs. 1 and 2, where the scattering data are compared with coupled channels calculations using the parameters of table 1. It should be noted that in comparison with ref. [12]) the overall normalization of the measured ^{3}He scattering cross sections has been reduced by 12 % on the basis of additional data not presented there.

The coupled channels calculations, represented by the solid lines in figs. 1 and 2, were carried out by coupling together the 0^+ ground state and the 2^+ and 4^+ members of the ground-state rotational band (data are available for the 0^+ and 2^+ levels only). The value of β_2 used in the calculations (0.28) is consistent with measurements for nuclei near $A \approx 165$, which also indicate that the hexadecapole parameter β_4 is

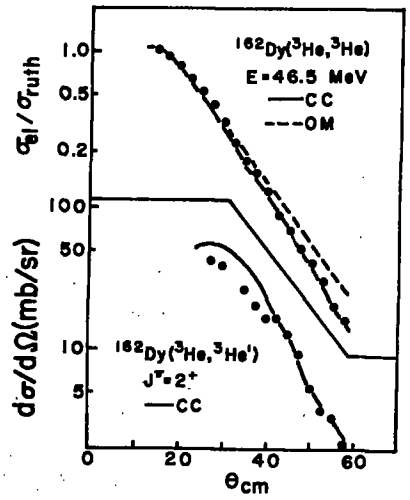

Fig. 1. Optical model and coupled channels predictions of ^{3}He scattering from ^{162}Dy at 46.5 MeV. Each calculation uses the potential parameters given in table 1.

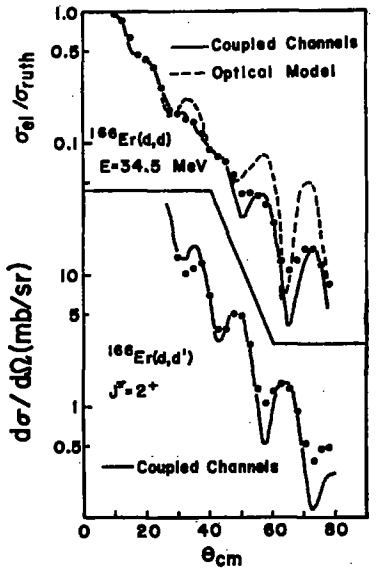

Fig. 2. Optical model and coupled channels predictions of deuteron scattering from ^{166}Er at 34.5 MeV. Each calculation uses the potential parameters given in table 1.

essentially zero [19]). Since the inclusion of a hexadecapole term in the potential with small values of β_4 had little effect on the predicted elastic and 2^+ cross sections, this term was dropped in the analysis presented here.

The dashed curves in figs. 1 and 2 show the result of dropping the coupling to the 2^+ and 4^+ levels, i.e., they give the pure optical model prediction. Clearly a good fit is not obtained; nevertheless it has been argued [see ref. [12]) and references therein] that these optical model parameters, which do fit elastic scattering from spherical nuclei, should be used in DWBA calculations. This procedure was found to give reasonable results in ref. [12]), and will be used here in making comparisons with the CCBA. The use in the DWBA calculations of optical potentials modified to fit the elastic scattering is not a feasible alternative here since it was not found possible to fit the deuteron scattering data with reasonable parameter sets. For further discussion of this problem see Ascuitto *et al.* [11]).

Except for a few examples noted in the text, the CCBA calculations employed the deformed Woods-Saxon (DWS) form factors discussed in the next section. Coriolis mixing and pairing effects occurring within a single band were included using the procedure described there. In addition appreciable band mixing could in principle lead to interband transitions in the exit channel due to inelastic de-excitation between bands. However, due to computing time limitations we were unable to include two (or more) Coriolis mixed bands. The largest effects from this omission would be

expected for the $\frac{1}{2}^+[411]$ and $\frac{3}{2}^+[411]$ bands, which are mixed fairly strongly by the Coriolis interaction and are known [20]) to have enhanced interband transition rates.

3. Form factors

In stripping reactions the nuclear structure information is specified by the overlap integral (ψ_B, ψ_A), where ψ_A and ψ_B are the wave functions of the initial and final states. The CCBA description of a single transition requires several such overlaps, one for each initial and final state pair, rather than the single one needed for the DWBA. For deformed nuclei this overlap can be written [2]) as

$$(\psi_B, \psi_A) = \left[\frac{2(2I_A+1)}{2I_B+1}\right]^{\frac{1}{2}} \sum_j \chi_{jm}(r)\langle I_A 0 j\Omega | I_B K_B\rangle\langle I_A M_A jm | I_B M_B\rangle, \qquad (3.1)$$

where $m = M_B - M_A$, K_A is assumed to be zero and $\chi_{jm}(r)$ is the angular momentum component j, m of the transferred particle with respect to the rotating core, with the label $K_B (= \Omega)$ suppressed.

A simple approximation to χ_{jm} would be the pure Nilsson wave function, i.e.,

$$\chi_{jm} = C_{lj}\varphi^{HO}_{Nljm}, \qquad (3.2)$$

where φ^{HO}_{Nljm} is a harmonic oscillator state and C_{lj} is the appropriate Nilsson coefficient. However, this is a poor approximation for reaction calculations because the slope of the radial wave function is incorrect in the tail region where the reactions occur. The conventional approach is to use

$$\chi_{jm} = C_{lj}\varphi^{WS}_{Nljm}, \qquad (3.3)$$

where φ^{WS}_{Nljm} is the eigenfunction of a spherical Woods-Saxon well, with the well depth adjusted to reproduce the separation energy and hence the correct radial slope outside the nuclear surface. A better procedure, discussed below, is to solve for the single-particle wave function in a deformed Woods-Saxon potential, which in some cases can be quite different from the simple prescription of eq. (3.3).

3.1. DEFORMED WOODS-SAXON FORM FACTOR CALCULATION

The Schrödinger equation for a proton moving in a deformed Woods-Saxon potential can be written

$$(H_0 + V')\psi_{E\Omega} = E\psi_{E\Omega}, \qquad (3.4)$$

where

$$H_0 = \frac{-\hbar^2}{2m}\nabla^2 + V(r) - \lambda\left(\frac{\hbar}{m_\pi c}\right)^2 \boldsymbol{L}\cdot\boldsymbol{\sigma}\frac{1}{r}\frac{dV}{dr} + V_C(r), \qquad (3.5)$$

Here V' is the potential due to deformation, $V_C(r)$ is the Coulomb potential of a uniformly charged sphere, and $V(r)$ is the usual spherical Woods-Saxon well:

$$V(r) = -V_0[1 + \exp(r - r_0)/a]^{-1}. \qquad (3.6)$$

We assume an axially symmetric, pure quadrupole deformation [experiment [19]) indicates a small value of β_4 near $A \approx 165$]. Each state is then specified by the energy E and Ω, the projection of the angular momentum on the symmetry axis, but can be conveniently labelled by Nilsson's asymptotic quantum numbers $\Omega^{\pi}[Nn_z\Lambda]$ appropriate to the $Z = 50$–82 region of interest.

The Woods-Saxon equipotentials are deformed while retaining constant volume (deformation of the Coulomb and spin-orbit potentials was not considered). To second order in the deformation parameter β_2 the result is [14])

$$V' = -\beta_2 Y_{20}(\theta) r \frac{\mathrm{d}V}{\mathrm{d}r} + \beta_2^2 \left\{ \left[Y_{20}(\theta) \right]^2 \left[r^2 \frac{\mathrm{d}^2 V}{\mathrm{d}r^2} + 2r \frac{\mathrm{d}V}{\mathrm{d}r} \right] + \frac{1}{4\pi} r \frac{\mathrm{d}V}{\mathrm{d}r} \right\}. \quad (3.7)$$

However, in the calculations to be reported here, the expansion (3.7) was extended to fourth order in β_2 since this was found necessary to obtain smooth, ellipsoidally shaped potentials. The fourth order expression is given by Rost [14]). The value of the deformation parameter β_2 was taken to be 0.28.

The eigenfunctions $\psi_{E\Omega}$ are expanded in angular momentum components

$$\psi_{E\Omega} = r^{-1} \sum_{l'j'} U_{El'j'\Omega'} |l'j'\Omega'\rangle. \quad (3.8)$$

Substituting (3.8) into (3.4) and taking the scalar product with $|lj\Omega\rangle$ leads to the set of coupled equations

$$(H_0 - E) U_{Elj\Omega} = -\sum_{l'j'} \langle lj\Omega | V' | l'j'\Omega \rangle U_{El'j'\Omega}. \quad (3.9)$$

for the radial functions $U_{Elj\Omega}$, from which the form factors are taken in the usual way.

Rost has described a relaxation technique by which eqs. (3.9) can be solved numerically in a reasonable time [14]). We have written a computer code [21]) based on his method which was used to supply form factors for the present analysis. These were computed with the constraint that the binding energy match the experimental value, thus ensuring the proper exponential tail. Given this constraint, eqs. (3.9) determine the well depth rather than the energy. An average binding energy was assumed for each state (i.e., each band). This should be a reasonable approximation since the rotational energy of the first few band members is of the order 100–200 keV compared with a total binding energy of about 5 MeV.

In addition to the required binding energy, it is also necessary to specify the radius and diffuseness of the potential (3.5), as well as the spin-orbit strength. Unfortunately there are ambiguities in the proper values for these parameters. As a reasonable, but not uniquely determined, basis for our comparison between the conventional (spherical) and deformed Woods-Saxon form factors, we have taken $r_0 = r_C = 1.25$ fm, $a = 0.63$ fm and $\lambda = 15$, where r_C is the radius parameter of the Coulomb potential. These values have been used, together with the (undeformed) optical potentials of table 1, in analyzing proton transfer reactions in the lead region [17]).

In figs. 3–5 we compare some of the deformed Woods-Saxon (DWS) functions with the conventional harmonic oscillator Woods-Saxon(HO-WS) form factors (the

latter are multiplied by the appropriate Nilsson coefficient, calculated in the usual harmonic oscillator basis). In cases where one angular-momentum component of a single-particle state is much larger than the others ($C_{lj} \approx 1$), there is little difference between the corresponding HO-WS and DWS functions, e.g., for the $j = \frac{11}{2}$ member of the $\frac{7}{2}^-$[523] state in ^{163}Ho (fig. 3). This is not the case for the weaker components or for *any* band member when the strength is more evenly divided, as for example in the $\frac{1}{2}^-$[541] band (fig. 4). Here the radial nodes are displaced and the tail is greatly enhanced except for the $\frac{7}{2}^-$ member (not shown), where it is diminished. Another effect is the appearance of an extra node in the DWS function for the higher angular momentum components of the $\frac{1}{2}^+$[411] and $\frac{3}{2}^+$[411] states (fig. 5). These can be qualitively understood as due to $\Delta N = 2$ mixing. A discussion of this point is given in the appendix.

3.2. CORIOLIS AND PAIRING EFFECTS

It is well known that the Coriolis and pairing interactions significantly modify the spectroscopic strengths for particle transfer reactions on deformed nuclei. These effects should properly be included in the set of coupled equations for the form factors. However, the Coriolis interaction (H_{RPC}) couples all of the particle orbitals within a major oscillator shell, which greatly complicates the solution of the coupled equations. No calculations of this type have been attempted.

If the Nilsson model is generalized to include pairing and Coriolis effects, the nuclear overlap integral for a single-nucleon stripping reaction has the form [2])

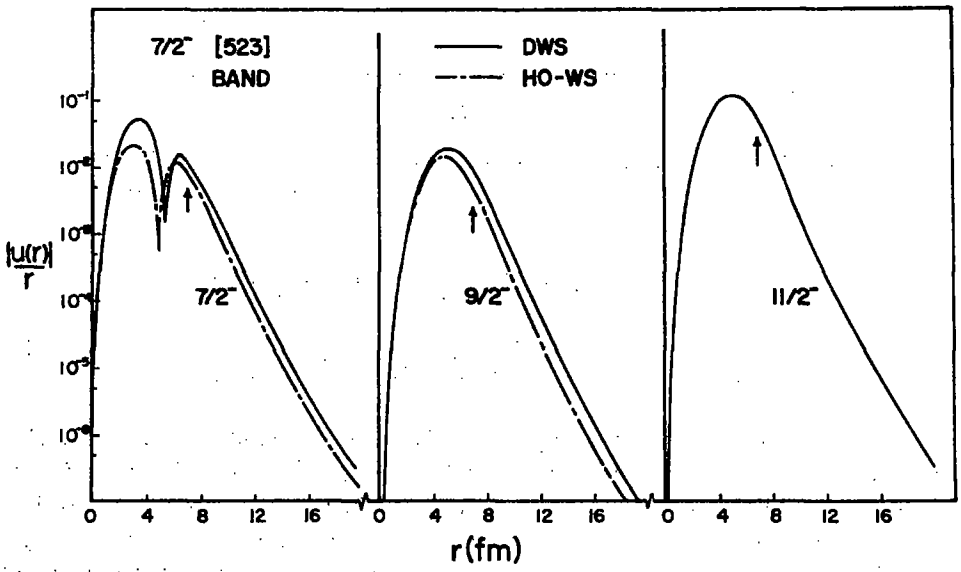

Fig. 3. Comparison of DWS and conventional HO-WS form factors for the first three members of the $\frac{7}{2}^-$[523] band in ^{163}Ho. The arrows denote the position of the potential radius, 1.25 $A^{\frac{1}{3}}$ fm.

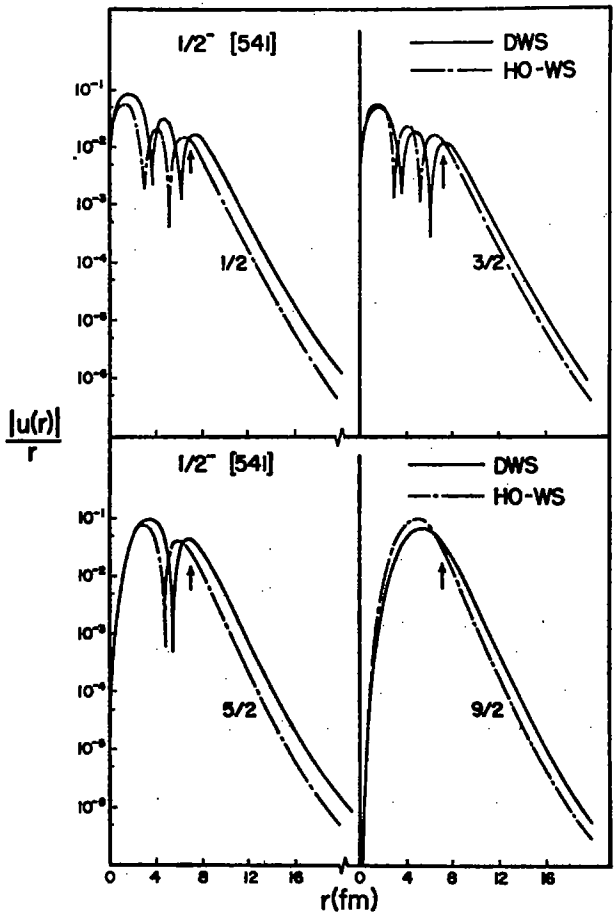

Fig. 4. DWS and the conventional HO-WS form factors for members of the $\frac{1}{2}^-$[541] band in ^{163}Ho. The arrows denote the position of the potential radius, 1.25 $A^{\frac{1}{3}}$ fm.

$$(\psi_B, \psi_A) = \sum_j \psi_{Nljm}(r) S_j^{B,A} \langle I_A M_A j (M_B - M_A) | I_B M_B \rangle$$

$$S_j^{B,A} = \left[\frac{2(2I_A+1)}{2I_B+1}\right]^{\frac{1}{2}} \langle I_A 0 j K_B | I_B K_B \rangle \sum_P a_P U_P C_{lj}^P, \tag{3.10}$$

where $S_j^{B,A}$ is the spectroscopic amplitude, U_P^2 is the probability that orbital P is unoccupied in the ground state of the target nucleus, C_{lj}^P is the Nilsson coefficient for orbital P, and the a_P are the Coriolis mixing coefficients. Since there is no explicit radial dependence in H_{RPC}, one would expect the redistribution of spectroscopic strength due to Coriolis mixing to be similar for a particle bound in either a deformed Woods-Saxon or a deformed harmonic oscillator potential. This assumption allows

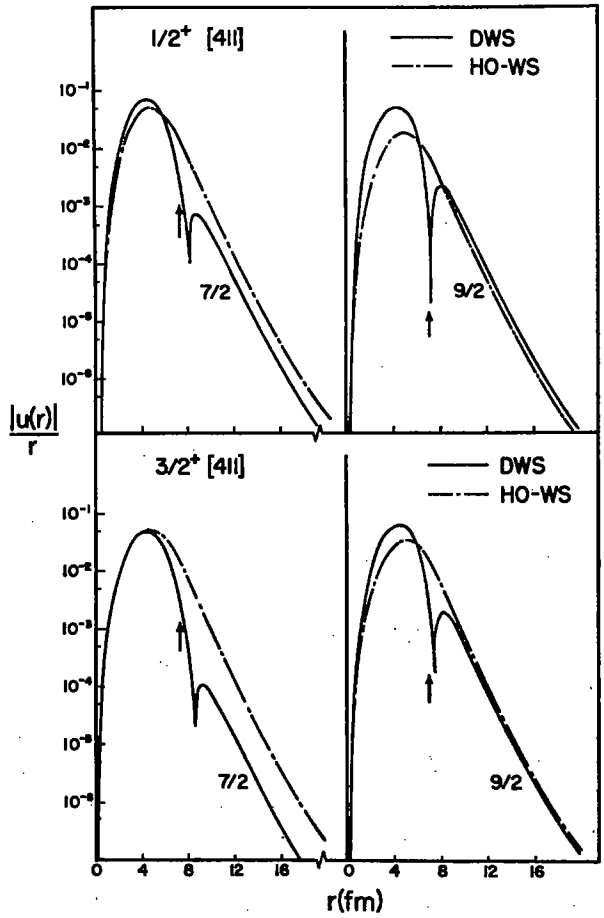

Fig. 5. The DWS and HO-WS form factors for the $\frac{7}{2}^+$ and $\frac{9}{2}^+$ members of the $\frac{1}{2}^+$[411] and $\frac{3}{2}^+$[411] bands, illustrating the appearance of extra nodes in the DWS functions due to $\Delta N = 2$ mixing. The arrows denote the position of the potential radius, 1.25 $A^{\frac{1}{3}}$ fm.

one to incorporate Coriolis and pairing effects into the reaction calculations through the substitution

$$\varphi_{Nljm}(r) \to [(1/C_{lj}) \sum_P a_P U_P C_{lj}^P] \chi_{jm}(r),$$
$$S_j^{B,A} \to [2(2I_A+1)/(2I_B+1)]^{\frac{1}{2}} \langle I_A 0 j K_B | I_B K_B \rangle, \tag{3.11}$$

where $\chi_{jm}(r)$ is a deformed Woods-Saxon wave function generated by the relaxation method outlined in subsect. 2.1. Except for a few cases specified in the text, this substitution was used in all the CCBA calculations.

The Coriolis and pairing calculations have been described previously [12]) and are briefly reviewed here. The Nilsson coefficients C_{lj}^P were calculated with the harmonic oscillator parameters δ, κ and μ set equal to 0.25, 0.05 and 0.625, respec-

tively. The values of the emptiness parameter U_p were computed in the usual BCS approximation with the gap parameter taken to be 850 keV and the chemical potential placed 100 keV below the ground state. For states which exhibited strong Coriolis mixing, the unmixed excitation energies were adjusted so that the resulting excitation energies would be correct when Coriolis effects were included.

It has been found [22]) that in many cases fits to experimental data can be improved by reducing the strength of the Coriolis interaction. In this work no such reductions were used.

4. Comparison with experiment

In our analysis of the ^{162,164}Dy(^{3}He, d)^{163,165}Ho reactions we have limited our attention to the low-lying bands for which transitions to at least one member were observed in each of the two residual nuclei. These include the ground $\frac{7}{2}^-$[523] band, as well as those based on the $\frac{1}{2}^+$[402], $\frac{1}{2}^+$[411], $\frac{3}{2}^+$[411], and $\frac{1}{2}^-$[541] orbitals. The "fingerprint" for the first two of these is dominated by a single strong transition which one might expect to be relatively well described by the DWBA, while for the remaining three the strength is fragmented and in addition the two [411] orbitals are Coriolis mixed. Thus these examples span a representative range of reaction conditions to be expected in similar experiments.

For most of the observed transitions the CCBA angular distributions are similar in shape to DWBA predictions, and are in good agreement with experiment over the 0–35° angular range for which data are available. In these cases the influence of indirect processes and the DWS form factors is manifested primarily in the cross-section *magnitudes*. For this reason the CCBA predictions displayed in the figures are *not* normalized to the data, except where noted. For comparison we also show DWBA calculations using the same optical parameters and HO-WS form factors which are normalized to Nilsson model predictions corrected for Coriolis and pairing effects. We emphasize that since these DWBA calculations do not use the DWS form factors and the one-channel optical potentials do not fit the elastic scattering, they do not necessarily represent the optimum description of the reactions obtainable with the DWBA. However we feel that they are representative of the conventional DWBA analyses which have commonly been used to extract spectroscopic information from proton-transfer reactions in the rare earth region.

The states of the target and residual nuclei included in the CCBA calculations are indicated explicitly in the figures. In the entrance channel the coupling always included three levels, the 0^+ ground state and the lowest 2^+ and 4^+ levels. In the exit channel as many levels were included as were likely to be important, bearing in mind computer time limitations.

4.1. THE $\frac{7}{2}^-$[523] and $\frac{1}{2}^+$[402] BANDS

These bands are similar in that almost all the spectroscopic strength of each resides in one member. Consequently one might expect the DWS and HO-WS form

factors to be similar, and the effect of indirect processes to be minimized, in the strong transitions to the $\frac{11}{2}^-$ member of the negative parity band and to the $\frac{5}{2}^+$[402] bandhead. For the $\frac{11}{2}^-$ level the DWS and HO-WS form factors are indeed nearly identical as is evident in fig. 3. Unfortunately, DWS form factors are not available for the $\frac{5}{2}^+$[402] band, as for this orbital the relaxation procedure always converged to a different band. However, the $\frac{5}{2}^+$ bandhead (the only member with an experimental cross section large enough to observe in either holmium isotope) is expected to carry approximately 90% of the spectroscopic strength of the band and should be adequately represented by the HO-WS form factor, which in this case was used in the CCBA calculations.

The experimental angular distributions for both the $\frac{11}{2}^-$ and $\frac{5}{2}^+$ levels are quite similar in the two holmium isotopes, as can be seen for example in comparing the $\frac{11}{2}^-$ angular distributions in fig. 6. For this transition the DWBA and CCBA are similar to one another and both fall within the experimental uncertainties of the data. For the $\frac{5}{2}^+$[402] bandhead, on the other hand, the experimental cross section is fitted quite well by the CCBA while the DWBA is too low by approximately a factor of two (fig. 7). Thus a significant contribution from indirect processes to this transition is indicated (as noted above, the two calculations use identical form factors for this

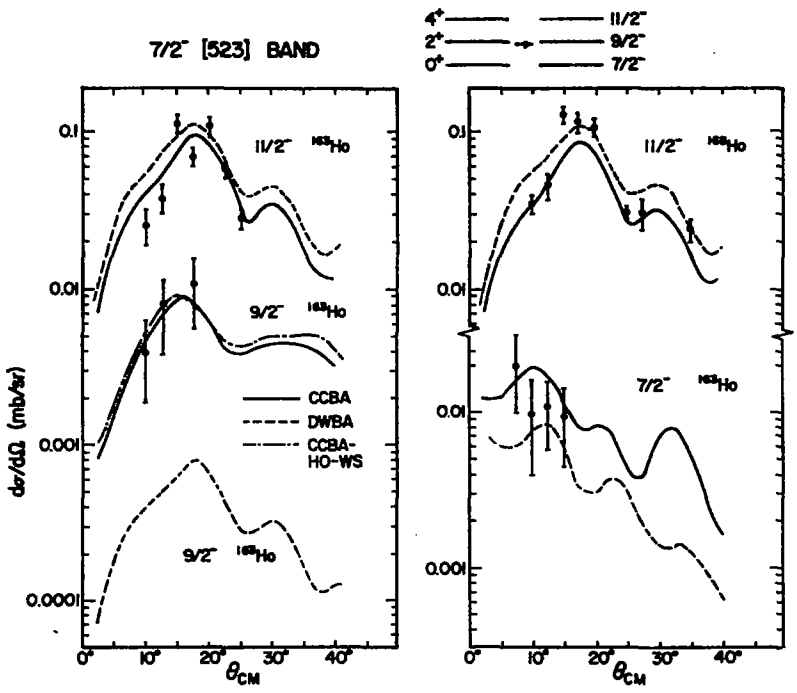

Fig. 6. Angular distributions for members of the $\frac{7}{2}^-$[523] band in ^{163}Ho and ^{165}Ho. The CCBA-HO-WS and DWBA calculations for the $\frac{9}{2}^-$ level use the same HO-WS form factor (see text).

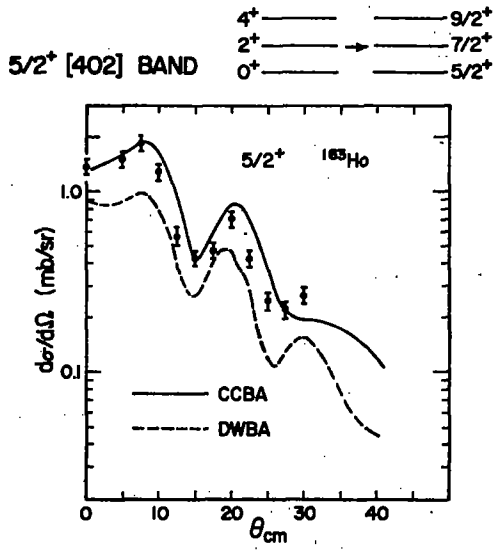

Fig. 7. Comparison of DWBA and CCBA predictions for the $\frac{5}{2}^+[402]$ bandhead in ^{163}Ho. The cross section for this transition in ^{165}Ho is similar [see ref. [12])].

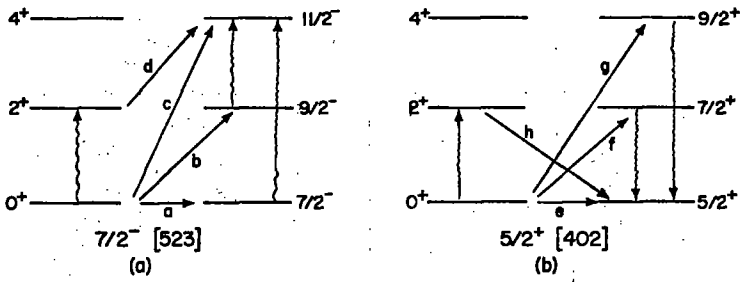

Fig. 8. First- and second-order paths which can contribute to excitation of the $\frac{11}{2}^-$ member of the $\frac{7}{2}^-[523]$ band (a) and the $\frac{5}{2}^+[402]$ bandhead (b).

orbital), even though it has the largest cross section measured in the ^{163,165}Ho experiments.

Some insight into the difference between these two cases can be gained by examining the spectroscopic amplitudes for second order processes, i.e., the ones which require exactly two steps. All of the paths for these are shown in fig. 8. For the $\frac{11}{2}^-$ transition (fig. 8a), only the direct path (c) and the path (d) through the target 2^+ state can proceed via the large $j^\pi = \frac{11}{2}^-$ transfer strength. (Recall that direct excitation of the 4^+ level is forbidden since β_4 is taken to be zero). However it happens that path (d) is inhibited by the angular momentum coupling, since the Clebsch-Gordan coefficient $\langle 20\ \frac{11}{2}\ \frac{7}{2} | \frac{11}{2}\ \frac{7}{2}\rangle$ is very small. Therefore, at least in second order, the direct route is favored due to this purely geometrical effect. The CCBA result, which also includes

the effects of multiple excitations and transfer via the weaker angular momentum components, is actually less than, but remains within about 15–20 % of, the purely direct cross section represented by the DWBA calculation. In the case of the transition to the $\frac{5}{2}^+$[402] bandhead, however, there is no similar geometrical hindrance of indirect contributions proceeding through the dominant component (in this case $j^\pi = \frac{5}{2}^+$) of the single-particle wave function. Of the relevant second-order paths for this transition (fig. 8b), only the path (h) through the 2^+ level in the entrance channel, in addition to the direct path (e), can proceed by $j^\pi = \frac{5}{2}^+$ transfer, and it appears that this path is responsible for much of the large cross-section enhancement predicted by the CCBA. Indeed, when all paths but (e) and (h) are turned off, the cross section predicted by the CCBA is within a few percent of the result with full coupling, i.e., the CCBA curve shown in fig. 7.

Among the weaker transitions populating the $\frac{7}{2}^-$[523] and $\frac{5}{2}^+$[402] bands, data are available only for the $\frac{7}{2}^-$ and $\frac{9}{2}^-$ members of the former in ^{163}Ho. The cross sections for these are also displayed in fig. 6. With the $\frac{9}{2}^-$ cross section we show the results of two CCBA calculations, together with the DWBA prediction. The curve labelled CCBA-HO-WS represents a coupled channels calculation using the HO-WS form factor (but without Coriolis corrections) rather than the DWS form factor used in the standard case. Although the measured cross section has large uncertainties it is evident that it is reproduced adequately by the two CCBA calculations while the DWBA underestimates the cross section by an order of magnitude.

The agreement between the two CCBA predictions is at first sight surprising in view of the large difference in the tail region between the $j^\pi = \frac{9}{2}^-$ DWS and HO-WS form factors (fig. 3). However, most of the observed cross section can be accounted for if excitation of the $\frac{9}{2}^-$ level is allowed to proceed only via indirect processes involving the stronger $\frac{11}{2}^-$ component, for which the DWS and HO-WS form factors are virtually identical. Such a CCBA calculation, with only $j^\pi = \frac{11}{2}^-$ transfer included, yields a cross section which at the first maximum near 15° is within about 10 % of two CCBA predictions shown in fig. 7.

For the $\frac{7}{2}^-$ member of this band the CCBA and DWBA predictions differ by more than a factor of two. However the experimental uncertainties are too large to indicate a preference for either.

4.2. THE $\frac{1}{2}^-$[541] BAND

In contrast to the orbitals considered in the previous subsection, most of the strength of this band is fragmented among four members, with $j^\pi = \frac{1}{2}^-, \frac{3}{2}^-, \frac{5}{2}^-$ and $\frac{9}{2}^-$. Data are available for each of the four in ^{163}Ho. For each of these levels the DWS form factors differ significantly from the conventional ones in that they are larger in the tail region. This effect, which is illustrated in fig. 4, can be understood from the fact that the $N = 7$ orbitals with which the $\frac{1}{2}^-$[541] can mix would not be bound in a spherical Woods-Saxon well of the appropriate radius and depth. Consequently some of the additional contributions appearing in the DWS form factors

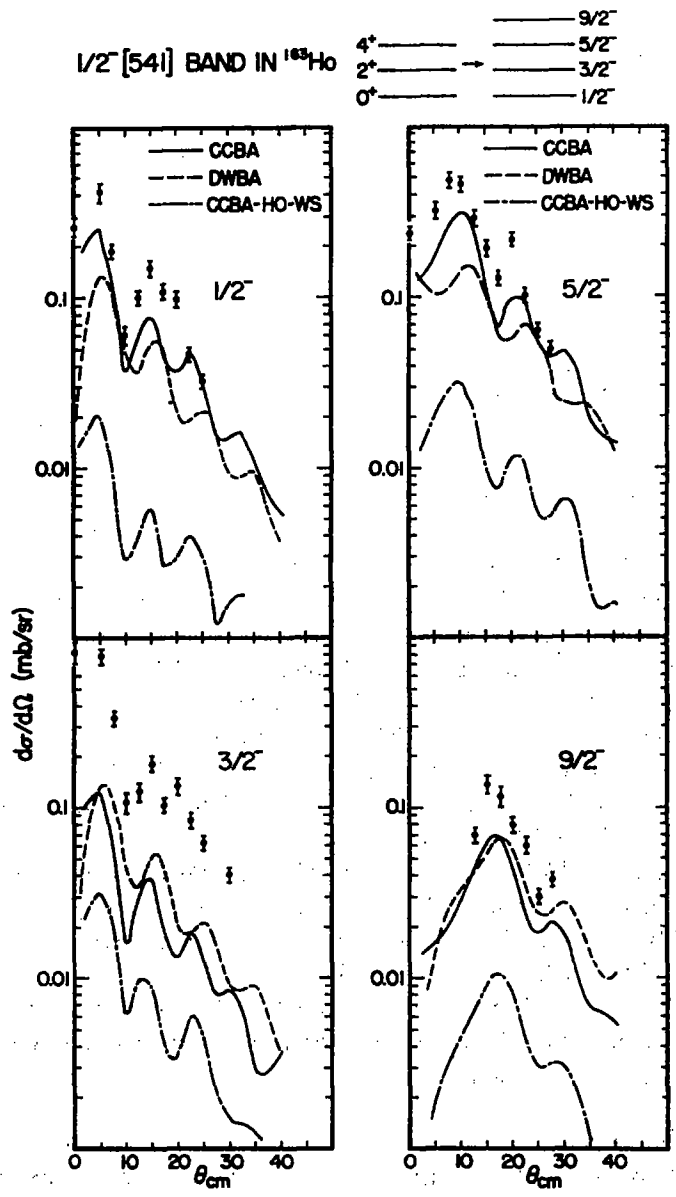

Fig. 9. Comparison of DWBA and CCBA predictions for members of the $\frac{1}{2}^-$[541] band in ^{163}Ho. The CCBA-HO-WS calculations use the same conventional form factor as the DWBA (see text).

are from the continuum, and for these four components add constructively, with a resulting extension of the functions to larger radii.

The experimental angular distributions are compared with DWBA and CCBA predictions in fig. 9. In each case the cross sections are underestimated. For the $\frac{1}{2}^-$

and $\frac{5}{2}^-$ levels, the CCBA falls approximately 35 % below the data while the DWBA is below the CCBA by about a factor of two. For the remaining two levels the CCBA and DWBA predictions are similar in magnitude but underestimate the $\frac{9}{2}^-$ cross section by a factor of two and the $\frac{3}{2}^-$ cross section by nearly an order of magnitude. Thus although the CCBA is more successful than the DWBA in reproducing the magnitudes of the experimental cross sections, the overall agreement is worse than for the other bands studied.

Two other members of this band, the $\frac{7}{2}^-$ and $\frac{11}{2}^-$ states, are predicted by the Nilsson model to have small direct-transfer strengths ($C_{ij}^2 \approx 0.03$ in each case). It is interesting that while the DWS function for the $\frac{11}{2}^-$ member is enhanced in the tail region relative to the HO-WS function by an amount roughly comparable to the $\frac{9}{2}^-$ component, the DWS function for the $\frac{7}{2}^-$ member is *diminished* by an order of magnitude near the nuclear surface. Thus for the latter the direct path would be expected to be quite small. Since neither level was identified in either ^{163}Ho or ^{165}Ho in the work of ref. [12]) no CCBA calculations have been made for these transitions.

It is noteworthy that for each of the four transitions considered the enhanced cross sections which might have been expected from the DWS form factors are suppressed by strong destructive interference appearing in the CCBA calculations. The rough similarity between the DWBA and CCBA cross sections results from approximate cancellation in the CCBA calculations of two strong but competing effects not present in the conventional DWBA. The strength of these two effects is illustrated by the broken curves marked CCBA-HO-WS in fig. 9. These represent CCBA calculations which use the conventional HO-WS form factors employed with the DWBA. (Since they do not include Coriolis corrections they are not strictly comparable to the other two sets of calculations, but this difference is a minor one.) It can be seen that the use of the DWS rather than HO-WS form factors results in a large enhancement of the cross sections (an order of magnitude for the $\frac{1}{2}^-$ and $\frac{5}{2}^-$ levels), which is counterbalanced by destructive interference among the multistep processes.

The presence of this strong interference between competing reaction processes, as well as the sensitivity of the reaction calculation to the form factor, indicates the danger of inferring detailed nuclear structure information from the usual "fingerprint" distribution of strengths. Even in cases for which the DWBA and CCBA cross sections are approximately the same, the nature of the "single-particle wave function" used in the two calculations can be quite different. Moreover, the large underestimates of the $\frac{3}{2}^-$ and $\frac{9}{2}^-$ strengths by both calculations renders suspect the relatively good agreement achieved for the other members of the band. Because of the interdependence between reaction channels implied by strong coupling, it is difficult to have confidence in the description of the intrinsic wave function unless the transitions to *all* members of the band are adequately reproduced.

In addition to the rather strong influence of indirect processes on the cross-section magnitudes for transitions populating the $\frac{1}{2}^-$[541] orbital, it is in this band that we find the only noticeable exceptions to the general trend that the shapes of the CCBA

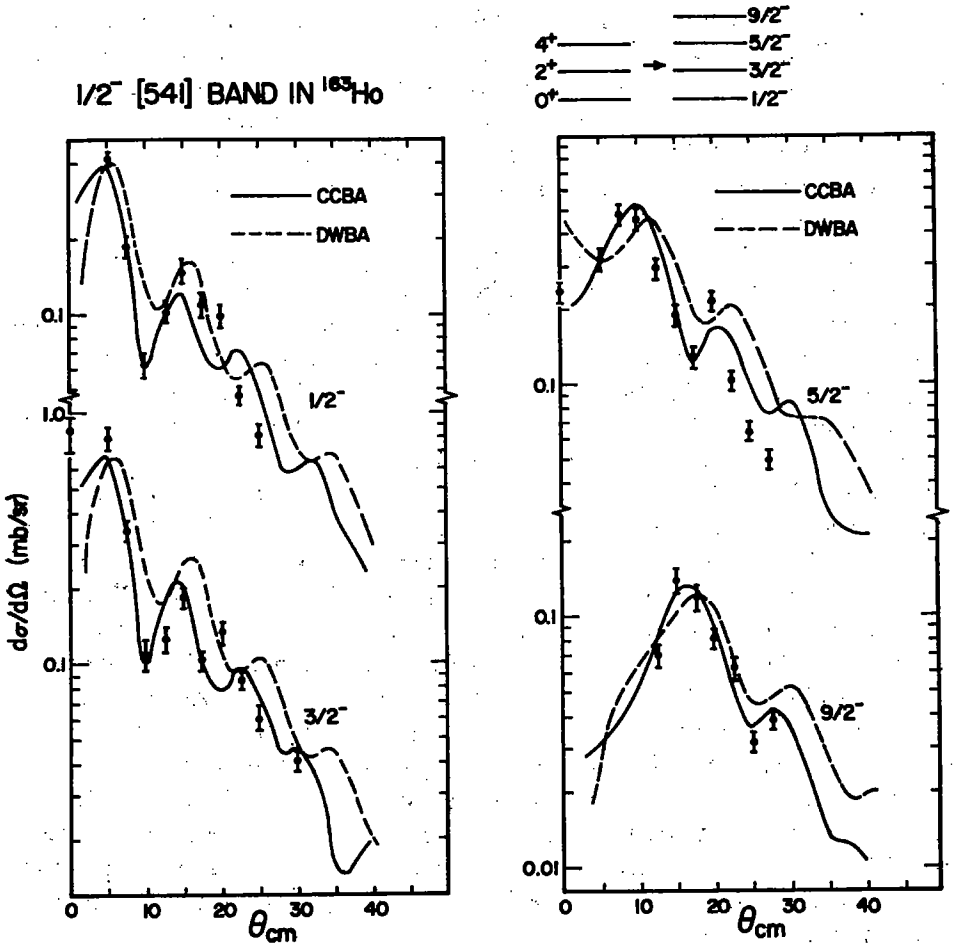

Fig. 10. Comparison of DWBA and CCBA angular distributions for transitions populating the $\frac{1}{2}^-$[541] band in ^{163}Ho. In each case the theoretical curves have been normalized to give the best visual fit to the data.

and DWBA angular distributions are quite similar and in good agreement with the data. In fig. 10 we compare the measured angular distributions with CCBA and DWBA predictions each of which have been normalized to give the best visual fit to the data. It can be seen that there are fairly large differences between the two calculations for the $l = 1$, $\frac{1}{2}^-$ and $\frac{3}{2}^-$ transitions, and while neither is successful in reproducing all the features the phase of the observed oscillations is somewhat better described by the CCBA. For the $l = 3, j^\pi = \frac{5}{2}^-$ transition there are again significant differences between the DWBA and CCBA, with the latter providing a distinctly better fit. For the relatively structureless $l = 5$ transition to the $\frac{9}{2}^-$ level, the differences are smaller and similar to those observed for transitions in other bands, although the CCBA gives a somewhat improved fit near the secondary maximum.

It will be recalled from the earlier discussion and fig. 4 that for the $\frac{1}{2}^-$[541] orbital the DWS form factors are quite different in shape from the HO-WS functions used in the DWBA calculation. However the altered radial dependence of the DWS form factors has little influence on the shape of the CCBA angular distributions. When these are calculated using the HO-WS form factors (see the curves marked CCBA-HO-WS in fig. 9), the resulting predictions are virtually identical in shape to those shown in fig. 10.

4.3. THE $\frac{1}{2}^+$[411] AND $\frac{3}{2}^+$[411] BANDS

The spectroscopic strength of both these bands is also distributed over several members, and as noted earlier there are indications in some of the DWS form factors of significant $N = 6$ contributions to the intrinsic wave function (see appendix and fig. 5). Thus one might expect to see appreciable departures from the predictions of the conventional DWBA. However, an element of uncertainty in treating the reactions populating these bands, and in comparing the calculations to the experimental data, is introduced by the strong Coriolis mixing between the two which is expected because of their close proximity in energy and which is borne out by the Coriolis mixing calculation described in subsect. 3.2.

We consider first the $\frac{1}{2}^+$[411] band. Experimental cross sections are available for the $\frac{3}{2}^+$, $\frac{5}{2}^+$ and $\frac{7}{2}^+$ members, which are expected to have most of the spectroscopic strength of the band. Unfortunately the $\frac{9}{2}^+$ level, which on the basis of the Nilsson model would have a small direct transfer strength ($C_{ij}^2 \approx 0.02$), was not identified in either holmium isotope in the (^{3}He, d) experiments (the predicted CCBA cross section is quite small, $\leq 2 \times 10^{-2}$ mb/sr at 10°). The $\frac{1}{2}^+$ level, with $C_{ij}^2 \approx 0.07$, was unresolved from the $\frac{3}{2}^+$ member in ^{163}Ho and from the $\frac{5}{2}\frac{1}{2}^+$[411] level in ^{165}Ho.

The available cross sections are compared with DWBA and CCBA predictions in fig. 11. The unresolved $\frac{1}{2}^+$-$\frac{3}{2}^+$ doublet in ^{163}Ho, which is expected to be dominated by the $\frac{3}{2}^+$ component, is compared with the combined predictions for these two levels. (At angles beyond 0° the weak $l = 0$ transition to the bandhead contributes less than 10 % to the predicted cross section.)

The CCBA and DWBA cross sections are similar in magnitude, and except for the $\frac{1}{2}^+$-$\frac{3}{2}^+$ doublet at forward angles, underestimate the experimental ones by about a factor of two. While the relatively poor agreement between experiment and theory may reflect uncertainties in the nuclear structure referred to earlier, the approximate agreement between the two types of calculation does not imply that indirect processes are unimportant in these transitions. In the case of the $\frac{7}{2}^+$ level the similarity between the DWBA and CCBA predictions is fortuitous, arising because of the difference between the DWS and HO-WS form factors used in the two calculations. This is illustrated by a second DWBA calculation, labelled DWBA-DWS in fig. 11, which uses the DWS form factor for the $\frac{7}{2}^+$ level. The diminished magnitude of this function in the tail region, compared with the HO-WS form factor used in the conventional DWBA (fig. 5), results in a reduction in the predicted cross section by a factor of four.

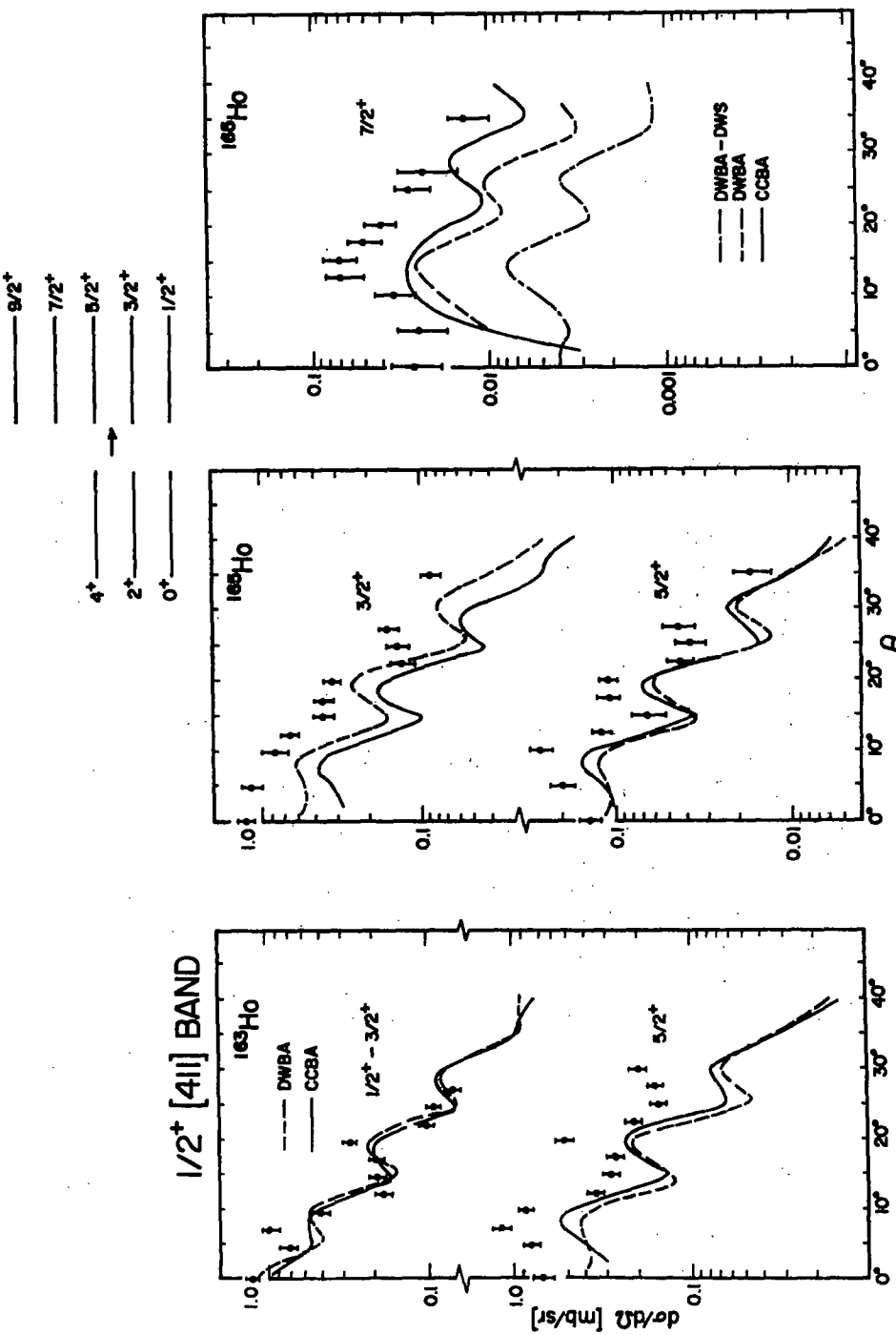

Fig. 11. Comparison of DWBA and CCBA predictions for members of the $\frac{1}{2}^+$ [411] band in ^{163}Ho and ^{165}Ho. The DWBA-DWS calculation for the $\frac{7}{2}^+$ level uses the same DWS form factor as the CCBA (see text).

However this reduction is more than erased by indirect contributions occurring in the CCBA calculation, which uses the DWS form factors. Thus the resulting CCBA prediction is similar to that of the HO-WS DWBA, although only a small part of the CCBA cross section is due to direct transfer. It is interesting to note that the additional node in the DWS form factors for this state changes the shape of the DWBA angular distribution, eliminating the sharp drop in the cross section near 0°, which does not appear in the data. However, in the full CCBA calculation the cross section again falls rapidly at forward angles.

In comparison with the $\frac{1}{2}^+$[411] band discussed above, somewhat less experimental information is available concerning the transitions populating the $\frac{3}{2}^+$[411] band. Although the positions of several members of this band are known in both ^{163}Ho and ^{165}Ho from decay work, only the bandhead in each isotope was clearly separated from other levels in the experimental spectra of Lewis *et al.* [12]), and only in ^{163}Ho was the cross section for this level large enough to observe. In addition, as mentioned earlier, a combined angular distribution for the strong $\frac{5}{2}^+$ component together with the weak $\frac{1}{2}^+$[411] bandhead transition was measured in ^{165}Ho.

The difference in the intensities of the reactions populating the $\frac{3}{2}^+$[411] bandhead in the two isotopes is only partly accounted for by the Coriolis mixing calculations, which enhance the expected cross section by a factor of five for the level in ^{163}Ho

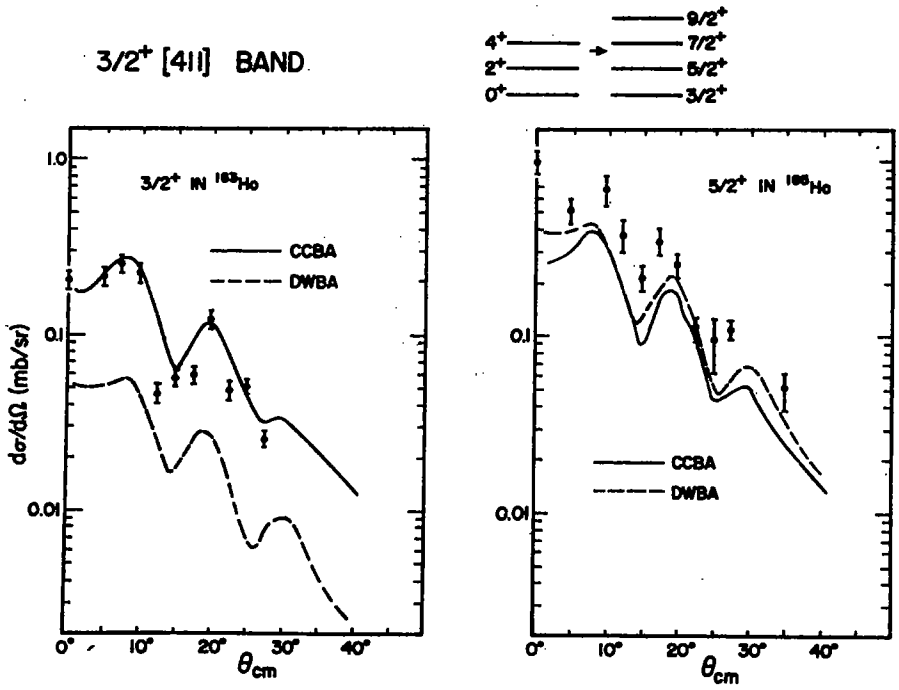

Fig. 12. DWBA and CCBA predictions for members of the $\frac{3}{2}^+$[411] band.

while diminishing the strength in ^{165}Ho. This predicted enhancement is reflected in the DWBA curve shown with the $\frac{3}{2}^+$ transition in ^{163}Ho (fig. 12), which nevertheless falls below the data by a factor of four. However the full CCBA calculation with the DWS form factor gives an excellent fit to the data. A similar calculation for the corresponding level in ^{165}Ho is consistent with the fact that in this isotope the transition was too weak to be observed. The predicted cross section at 10° is only 1.2×10^{-2} mb/sr. Although the much stronger $\frac{5}{2}^+$ transition was unresolved from the $\frac{1}{2}^+$[411] bandhead in ^{165}Ho, the latter is expected to contribute less than 10% of the combined cross section measured for the two levels. Assuming this contribution to be negligible, the DWBA and CCBA predictions are similar, each underestimating the data by not quite a factor of two. For the $\frac{5}{2}^+$ level in ^{163}Ho, the CCBA predicts a cross section approximately half that in ^{165}Ho. In this case no meaningful comparison with experiment is possible, since in this isotope the $\frac{5}{2}^+$ level is nearly degenerate with the strongly populated $\frac{7}{2}^+$[404] bandhead.

Among the unresolved higher spin members of this band, the $\frac{7}{2}^+$ member in ^{163}Ho is predicted by the Coriolis mixing calculations to have the largest direct transfer strength [$(\sum_p a^p U^p C_0^p)^2 \approx 0.07$]. However, as was the case for the $\frac{7}{2}$ $\frac{1}{2}^+$[411] level discussed earlier, indirect processes account for most of the CCBA cross section predicted for this level. As can be seen in fig. 5, the DWS form factor for the $\frac{7}{2}^+$ member is greatly diminished in the tail region compared with the HO-WS function. However the CCBA prediction using DWS form factors is some 2.4 times larger than the cross section predicted by the HO-WS DWBA. The predicted CCBA cross sections are nonetheless small; at 10°, 2×10^{-2} and 6×10^{-3} mb/sr in ^{163}Ho and ^{165}Ho, respectively. Comparable cross sections are predicted for the $\frac{9}{2}^+$ member; at 10°, 1×10^{-2} mb/sr in ^{163}Ho and 2×10^{-2} mb/sr in ^{165}Ho.

5. Summary and conclusions

For most of the transitions we have analyzed, the CCBA predicts significant contributions from indirect processes to the (^{3}He, d) reaction mechanism. The resulting influence on cross-section magnitudes, and on the pattern of spectroscopic strengths which would be inferred from a conventional DWBA analysis, is comparable in degree to that found in neutron transfer reactions in the rare-earth region at lower energies. These effects are not confined to weak transitions. Even for the very strongly populated $\frac{5}{2}^+$[402] bandhead, the CCBA cross section is enhanced by a factor of two over the DWBA. For the weaker transitions, the effect of the more realistic deformed Woods-Saxon form factors on the predicted cross section is sometimes comparable to the influence of indirect processes. Each can alter the cross section by an order of magnitude. In the limited number of examples we have considered, these effects tend to cancel, resulting in predicted cross sections which are often similar to those of the conventional DWBA. However since each can either

enhance or reduce the cross section in a way which is essentially unpredictable *a priori*, we see no reason why this behavior should be universal.

In most of the present examples, the CCBA angular distributions are quite similar to DWBA predictions, which usually fit the data well. Thus the DWS form factors and the indirect reaction paths included in the CCBA model manifest themselves mainly in altered cross-section magnitudes. In this respect the CCBA results are in better overall agreement with experiment than the DWBA as applied by Lewis *et al.* [12]). However there remain some major discrepancies, all in the $\frac{1}{2}^-$[541], $\frac{1}{2}^+$[411] and $\frac{3}{2}^+$[411] bands. For the majority of transitions to members of these three bands, the CCBA cross sections, although usually larger than the DWBA predictions, still underestimate the experimental cross sections by nearly a factor of two. The strongest inelastic effects, and some of the largest discrepancies, occur in the $\frac{1}{2}^-$[541] band, where there are also noticeable differences between the CCBA and DWBA angular distributions. Here the CCBA is more successful in reproducing both the shapes and magnitudes of the experimental angular distributions, although it fails badly in predicting the strength of the transition to the $\frac{3}{2}^-$ level and underestimates the cross sections for the other members of the band. Because of the strong interference occurring in the CCBA calculations for the $\frac{1}{2}^-$[541] band, one might expect the cross sections to be particularly sensitive to nuclear structure details, and it may be that the relatively poor agreement obtained for this orbital, as well as for the two Coriolis-mixed [411] bands, is due at least in part to uncertainties in the underlying nuclear structure. However it is curious that when significant discrepancies exist, the CCBA cross sections are always smaller than the experimental ones, and usually by roughly the same factor. Indeed we note that of the eleven transitions to the members of these three bands shown in figs. 9, 11 and 12, the experimental cross sections for all but the $\frac{3}{2}$ $\frac{1}{2}^-$[541] and $\frac{3}{2}$ $\frac{3}{2}^+$[411] levels can be reproduced to within about 20 % if the CCBA predictions are uniformly multiplied by a factor of 1.9.

There is of course some uncertainty in the proper overall normalization of the predicted cross sections, which depends upon the normalization factor D_0^2 assumed for the (^{3}He, d) reaction [15]). In addition the absolute cross sections yielded by the calculations are subject to uncertainties in parameters, such as the radius of the bound-state potential, whose variation tends to affect the cross-section magnitudes for all transitions in roughly the same way. However even if one accepts a possible error of as large as 1.9 in the effective overall normalization due to these uncertainties, a uniform renormalization of this magnitude would be difficult to justify in the present case. The result would be to destroy the very good agreement obtained for the $\frac{7}{2}^-$[523] and $\frac{5}{2}^+$[402] orbitals, which among the examples we have analyzed are probably subject to the smallest nuclear structure uncertainties.

Thus the present CCBA analysis, although indicating that spectroscopic strengths obtained from the usual DWBA procedure can be substantially in error, is not itself able to reproduce quantitatively the experimental cross-section magnitudes for all transitions. It is difficult to say, based on the limited number of cases considered

here, whether the discrepancies between this more elaborate reaction model and experiment reflect the various uncertainties in parameters and nuclear structure or more fundamental deficiencies in the description of the reaction. It is our feeling that this question would only be resolved by the systematic analysis of a more extensive body of data.

One of us (A.S.B.) would like to thank Dr. P. E. Hodgson for the hospitality extended to him during a visit to Oxford.

Appendix

MIXING BETWEEN MAJOR OSCILLATOR SHELLS

In general, shell-model states with quantum numbers $N+2$, l, j have one more radial node than those with quantum numbers N, l, j, suggesting that the additional nodes which appear in some DWS form factors are due to $\Delta N = 2$ mixing. This point is difficult to investigate using Woods-Saxon basis states because in the spherical limit the states with $N+2$ are usually unbound in a potential which puts members of the major shell N near the Fermi surface. However it is straightforward to investigate using harmonic oscillator functions. In terms of these the additional nodes in the DWS form factors can be understood as arising from $\Delta N = 2$ mixing and it is possible to anticipate the cases in which they occur.

Consider a case in which the single particle state is an admixture of $N = 4$ and $N = 6$ harmonic oscillator basis states. The number and positions of the radial nodes then depend on the mixing ratio $C(N = 6)/C(N = 4)$. If the wave function were pure $N = 4$, there would be $N-\frac{1}{2}l$ radial nodes. The existence of an additional node in the mixed wave functions is determined by the following conditions. (We assume the usual phase convention, in which the radial wave function is positive near the origin.)

(a) If the mixing ratio is positive, there will always be an additional node whose position approaches infinity as the mixing ratio $C(N = 6)/C(N = 4)$ approaches zero, since the $N = 6$ wave function must dominate at sufficiently large r. Conversely, as $C(N = 6)/C(N = 4)$ approaches infinity, the additional node moves in significantly while the existing nodes move slightly closer to the origin.

(b) If the mixing ratio is negative, there will be an additional node only if the magnitude of the mixing ratio is sufficiently large. The additional node moves toward the origin and disappears at $C(N = 6)/C(N = 4)$ becomes small. The existing nodes move away from the origin as $C(N = 6)/C(N = 4)$ approaches negative infinity.

These statements are valid for any admixture of N and $N+2$ harmonic oscillator wave functions. They depend on only two properties of the wave functions, namely, that the radial nodes of the N and $N+2$ wave functions interlace each other and that the ratio of the radial wave functions $(\varphi^N/\varphi^{N+2})$ approaches zero as r approaches infinity.

These considerations are best illustrated by the behaviour of the $\frac{1}{2}^+[411]$ and $\frac{3}{2}^+[411]$ Nilsson states, which are among those populated by the (^{3}He, d) reactions of interest. In a deformed harmonic oscillator potential with parameters appropriate for the holmium isotopes, these two states have energies (before $\Delta N = 2$ mixing) very close to their $N = 6$ partners, the $\frac{1}{2}^+[660]$ and $\frac{3}{2}^+[651]$ orbitals. Thus conditions are favorable for such mixing to occur. The predicted mixing ratios $C(N = 6)/C(N = 4)$ for the first few members of each band are given in table 2 for two values of the deformation, $\delta = 0.2$ and $\delta = 0.3$ (for ^{163,165}Ho an intermediate value $\delta \approx 0.23$ is reasonable). The mixing ratios were computed with the deformed oscillator parameters taken to be $\kappa = 0.05$, $\mu = 0.625$, the values recommended by Chi [22]), and $\hbar\omega_0 = 7.3$ MeV. Also in the table we compare the nodal character of the mixed harmonic oscillator functions with that of the corresponding DWS form factors.

TABLE 2

Comparison of DWS functions with $\Delta N = 2$ mixing ratios and nodal positions predicted using a harmonic oscillator basis

State	Component	Harmonic oscillator				DWS
		$\delta = 0.2$		$\delta = 0.3$		existence of extra node
		$C(N = 6)/C(N = 4)$	position extra node (fm)	$C(N = 6)/C(N = 4)$	position extra node (fm)	
$\frac{1}{2}^+[411]$	$\frac{1}{2}$	−0.062	none	−0.096	none	no
	$\frac{3}{2}$	−0.072	none	−0.112	none	no
	$\frac{5}{2}$	0.047	20	0.017	$\gg 20$	no
	$\frac{7}{2}$	0.251	9	0.302	9	yes
	$\frac{9}{2}$	0.692	7	0.780	7	yes
$\frac{3}{2}^+[411]$	$\frac{3}{2}$	−0.109	none	−0.143	none	no
	$\frac{5}{2}$	−0.030	none	−0.061	none	no
	$\frac{7}{2}$	0.113	12	0.156	11	yes
	$\frac{9}{2}$	0.569	7	0.663	7	yes

In all cases but one the harmonic oscillator and DWS functions have the same number of nodes. The exception is the $j = \frac{1}{2}$ component of the $\frac{1}{2}^+[411]$ state, which in the oscillator potential has an extra node at or beyond 20 fm which does not appear in the DWS function. This is reasonable, since at radii far beyond the finite extent of the Woods-Saxon well the wave function must be an exponentially decaying Coulomb function.

It should be emphasized that although the study of $\Delta N = 2$ mixing in a harmonic oscillator basis enables one to predict when there may be changes in the number of nodes, it is not clear what effect this will have on the tails of the wave functions. For example both the $\frac{7}{2}$ and $\frac{9}{2}$ components of the $\frac{1}{2}^+[411]$ band have positive mixing ratios and additional radial nodes, but in one case the tail is enhanced and in the other it is diminished (see fig. 5).

References

1) G. R. Satchler, Ann. of Phys. **3** (1958) 275
2) B. Elbek and P. O. Tjøm, in Advances in nuclear physics, vol. 3, ed. M. Baranger and E. Vogt (Plenum Press, NY, 1969)
3) S. K. Penney and G. R. Satchler, Nucl. Phys. **53** (1964) 145
4) R. J. Ascuitto and N. K. Glendenning, Phys. Rev. **181** (1969) 1396
5) D. J. Edens, Thesis (1970) Oxford University
6) D. Braunschweig, T. Tamura and T. Udagawa, Phys. Lett. **35B** (1971) 273;
   A. K. Abdallah, T. Udagawa and T. Tamura, Phys. Rev. **C8** (1973) 1855
7) P. J. Ellis and A. Dudek, Particles and Nuclei **5** (1973) 1;
   T. Vertse, A. Dudek-Ellis, P. J. Ellis, T. A. Belote and D. Roaf, Nucl. Phys. **A223** (1974) 207
8) N. K. Glendenning and R. S. Mackintosh, Nucl. Phys. **A168** (1971) 575
9) H. Schulz, H. J. Wiebicke and F. A. Gareev, Nucl. Phys. **A180** (1972) 625
10) R. J. Ascuitto, C. H. King and L. J. McVay, Phys. Rev. Lett. **29** (1972) 1106;
   L. J. McVay, R. J. Ascuitto and C. H. King, Phys. Lett. **43B** (1973) 119
11) R. J. Ascuitto, C. H. King, L. J. McVay and B. Sørensen, Nucl. Phys. **A226** (1974) 454
12) D. A. Lewis, A. S. Broad and W. S. Gray, Phys. Rev. **C10** (1974) 2286
13) P. E. Nemirovsky and V. A. Chepurnov, Sov. J. Nucl. Phys. **3** (1966) 730;
   B. L. Anderson, B. B. Back and J. M. Bang, Nucl. Phys. **A147** (1970) 33
14) E. Rost, Phys. Rev. **154** (1967) 994
15) R. H. Bassel, Phys. Rev. **149** (1966) 791
16) P. D. Kunz, Computer program DWUCK (1967), University of Colorado, unpublished
17) W. C. Parkinson, D. L. Hendrie, H. H. Duhm. J. Mahoney, J. Saundinos and G. R. Satchler, Phys. Rev. **178** (1969) 1976
18) F. Hinterberger, G. Mairle, U. Schmidt-Rohr, G. J. Wagner and P. Turek, Nucl. Phys. **A111** (1968) 265
19) D. L. Hendrie, N. K. Glendenning, B. G. Harvey, D. N. Jarvis, H. H. Duhm, J. Saundinos and J. Mahoney, Phys. Lett. **26B** (1968) 127
20) G. Mauron, J. Kern and O. Huber, Nucl. Phys. **A181** (1972) 489;
   L. Funke, K. H. Kaun, P. Kemnitz, H. Sodan and G. Winter Nucl. Phys. **A190** (1972) 576
21) A. S. Broad, Thesis (1974), University of Michigan
22) M. E. Bunker and C. W. Reich, Rev. Mod. Phys. **43** (1971) 348
23) B. E. Chi, Nucl. Phys. **83** (1966) 87